SCIENCE CHINA
Chemistry

• ARTICLES •
• SPECIAL ISSUE • Organic photovoltaics

February 2015 Vol.58 No.2: 267–275
doi: 10.1007/s11426-014-5223-7

Low band-gap benzodithiophene-thienothiophenecopolymers: the effect of dual two-dimensional substitutions on optoelectronic properties

Zhulin Liu, Jiangman Sun, Yongxiang Zhu, Peng Liu, Lianjie Zhang*, Junwu Chen*, Fei Huang & Yong Cao

Institute of Polymer Optoelectronic Materials and Devices, State Key Laboratory of Luminescent Materials and Devices, South China University of Technology, Guangzhou 510640, China

Received July 28, 2014; accepted August 18, 2014; published online December 25, 2014

Two new conjugated copolymers, PBDT-T6-TTF and PBDT-T12-TTF, were derived from a novel 4-fluorobenzoyl thienothiophene (TTF). In addition, two types of benzodithiophene (BDT) units with 2,3-dihexylthienyl (T6) and 2,3-didodecylthienyl (T12) substituents, respectively, were successfully synthesized. The effect of the dual two-dimensional (2D) substitutions of the building blocks upon the optoelectronic properties of the polymers was investigated. Generally, the two polymers exhibited good solubility and broad absorption, showing similar optical band gaps of ~1.53 eV. However, PBDT-T6-TTF with its shorter alkyl chain length possessed a larger extinction coefficient in thin solid film. The highest occupied molecular orbital (HOMO) level of PBDT-T6-TTF was located at –5.38 eV while that of PBDT-T12-TTF was at –5.51 eV. In space charge-limited-current (SCLC) measurement, PBDT-T6-TTF and PBDT-T12-TTF displayed respective hole mobilities of 3.0×10^{-4} and 1.6×10^{-5} cm^2 V^{-1} s^{-1}. In polymer solar cells, PBDT-T6-TTF and PBDT-T12-TTF showed respective power conversion efficiencies (PCEs) of 2.86% and 1.67%. When 1,8-diiodooctane (DIO) was used as the solvent additive, the PCE of PBDT-T6-TTF was remarkably elevated to 4.85%, but the use of DIO for the PBDT-T12-TTF-blend film resulted in a lower PCE of 0.91%. Atomic force microscopy (AFM) indicated that the superior efficiency of PBDT-T6-TTF with 3% DIO (*v*/*v*) should be related to the better continuous phase separation of the blend film. Nevertheless, the morphology of the PBDT-T12-TTF deteriorated when the 3% DIO (*v*/*v*) was added. Our results suggest that the alkyl-chain length on the 2D BDT units play an important role in determining the optoelectronic properties of dual 2D BDT-TT-based polymers.

conjugated copolymers, benzodithiophene, thienothiophene, dual 2-dimentional substitutions, alkyl side-chain length

1 Introduction

Low-band-gap conjugated polymers, one branch of functional polymers, have attracted widespread attention from scientific communities because of their important applications as photoactive donors in bulk-heterojunction polymer solar cells (BHJ PSCs), which are important in low-cost green-energy utilization [1–4]. Among the various polymer donors, alternating copolymers based on benzo[1,2-*b*:4,5-*b*′] dithiophene (BDT) and thienothiophene (TT) have become the most promising candidates; reports have also been made on the energy-conversion efficiency of BHJ PSCs [5–10].

Conjugated polymers normally comprise very rigid backbones, which means that introductions of suitable side-chains onto the building blocks of the conjugated polymers are required to achieve enough solubility for their solution-processing [11]. So far, long alkyl or alkoxyl groups have been widely utilized as the typical side-chains for a variety of conjugated polymers [12,13]. In addition, the

*Corresponding authors (email: lianjiezhang@scut.edu.cn; psjwchen@scut.edu.cn)

electronic properties of conjugated polymers could be tuned through the different electron-donating effects of alkyl or alkoxy groups and/or their indirect effects via their aggregation ability on the polymer main chain [13–15].

As for the family of the BDT-TT-based polymer donor, early efforts on the structural modification of the repeating unit have been made by changing the aliphatic side-chain. For example, in 2009, Yu *et al*. [16] varied the aliphatic side-chains on both the BDT and TT units and showed that suitable aliphatic groups were of great importance for the optimization of the polymer donors. In the same year, Yang and Hou *et al.* [6] modified the TT unit through the replacement of the alkoxycarbonyl group with the alkylcarbonyl group, which led to a V_{oc} value of 0.7 V and a high power conversion efficiency (PCE) of as much as 6.58%.

Further optimizations of BDT [17–21] have attracted more and more attention in order to obtain better photovoltaic performance from the BDT-TT-based polymer family. Two-dimensional (2D) side-chains containing aromatic rings rather than aliphatic chains only have been extensively exploited to further adjust the electronic properties of BDT-based polymer donors with better photovoltaic performances. Therefore, the selection of 2D pendants on a BDT unit is extremely significant because of the varied aromatic rings and their different substituted aliphatic chains. In 2011, Hou *et al.* [22] pioneered such research by synthesizing a 2D BDT unit using a 2-ethylhexyl-5-thienyl group and a polymer bearing alkylcarbonyl-substituted TT. The polymer exhibited a higher V_{oc} of 0.74 V and an improved efficiency of 7.59%. In 2013, Hwang *et al.* [23] investigated the effect of the 2-ethylhexyl-5-thienothienyl pendant on the polymer backbone; their work demonstrated that the polymer with the fused 2D side-chain was prone to face-on orientation and hence achieved ahigh efficiency of 7.71%. Very recently, Li and Wong *et al.* [24] studied three kinds of substitutions on the thienyl pendant and found that the polymer comprising the alkythiothienyl-substituted BDT with a fluorinated TT possessed the best efficiency, 8.42% with a V_{oc} of 0.84 V, in comparison to alkoxy and alkyl substitutions.

The stability of the quinoid form of TT is also crucial for the construction of BDT-TT-based polymer donors. Aside from the replacement of ester linkage with carbonyl linkage or sulfonyl linkage and the introduction of fluorine atoms [6,25–27], the 2D side-chain on the TT unit also has recently been developed [28,29]. In 2011, Ikai *et al.* [29] synthesized various 2D side-chains on a TT unit and demonstrated that the 4-substituted phenyl ester group with an electron-withdrawing group as a pendant not only deepened the highest occupied molecular orbital (HOMO) level of the related polymers but also slightly broadened the absorption. However, no photovoltaic performances of the 2D-TT-based polymers were reported. It should be noted that 2D-TT with a carbonyl linkage has not been reported either.

In this work, we designed both BDT and TT units toward 2D structures whose 2,3-alkyl thienyl pendant was on the 2,6-positions of the BDT unit and the 4-fluoro-benzoyl group was on the 2-position of TT unit (TTF) (Scheme 1). The dual 2D building blocks of the repeating unit may supply the synergistic effects of lowering the HOMO level of the resulting polymers and narrowing their optical bandgaps. To date, long alkyl side-chains have been widely utilized to enhance solubility, strengthen intermolecular interaction, and allow high hole mobility [13,30]. We therefore chose two different 2,3-dialkyl thienyl pendants, 2,3-dihexylthienyl (T6) and 2,3-didodecylthienyl (T12) in order to elucidate the influence of the alkyl chain length on the device performance. The two new polymers, PBDT-T6-TTF and PBDT-T12-TTF, exhibited deep HOMO levels of –5.38 eV and –5.51 eV, respectively, which suggests that the longer the alkyl chain, the deeper the HOMO level. Although the absorption ranges of the two polymers were comparable from ~300 to more than 800 nm, the maximum extinction coefficient for PBDT-T6-TTF was twice that of PBDT-T12-TTF, which indicated their different aggregation abilities. It was found that DIO could greatly affect the morphologies of the active layers of the two polymers. With the DIO as a solvent additive, the PCE of PBDT-T6-TTF was elevated from 2.86% to 4.85%, whereas PBDT-T12-TTF-based PSCs showed decreased efficiency. Our results demonstrate that the dual 2D BDT-TT polymers could possess relatively deeper HOMO levels and broader absorption, and that the alkyl-chain length of the 2D BDT units would play an important role in determining the extinction coeffi-

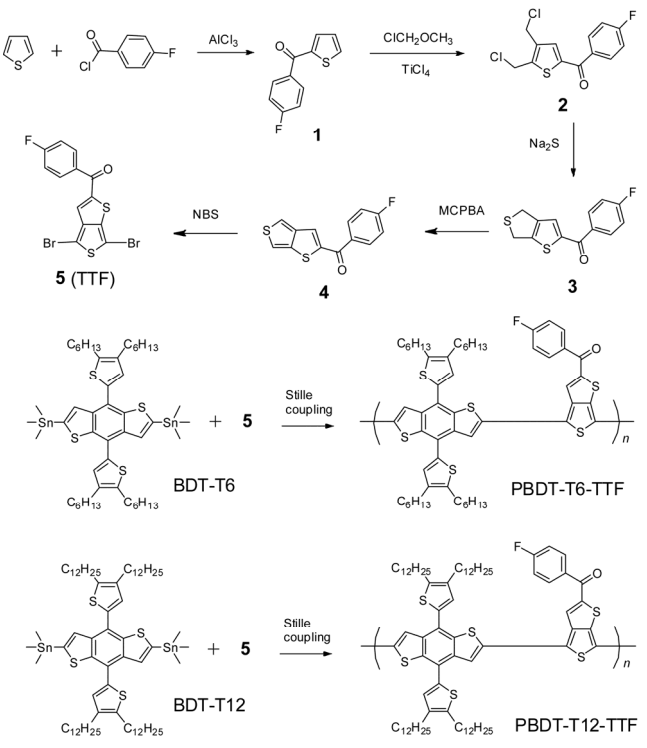

Scheme 1 Synthesis of the TTF and the polymers.

cient and hole mobility of pristine polymer film as well as the morphology of its blend film.

2 Experimental

2.1 Materials and instrumentations

All reagents solvents, unless otherwise specified, were obtained from Aldrich (Shanghai), Acros (Beijing), and TCI Chemical Co. (Japan) and were used as received. Anhydrous tetrahydrofuran was distilled over sodium/benzophenone under N_2 prior to use. All manipulations involving air-sensitive reagents were performed under an atmosphere of dry argon. The 2,6-Bis(trimethyltin)-4,8-di(2,3-dihexylthiophen-5-yl)-benzo-[1,2-*b*:4,5-*b′*]dithiophene (BDT-T6) and 2,6-bis(trimethyltin)-4,8-di(2,3-didodecyl-thiophen-5-yl)-benzo[1,2-*b*:4,5-*b′*]dithiophene (BDT-T12) were prepared similarly, according to the literature [22], and both were recrystallized to reach the desirable purity for polymerization.

^{1}H NMR spectra were recorded on Bruker AV 300 and 600 spectrometers (Switzerland) with tetramethylsilane (TMS) as the internal reference. Molecular weights of the polymers were obtained on a Waters GPC 2410 (England) using a calibration curve of polystyrene standards, with tetrahydrofuran as the eluent. Elemental analyses were performed on a Vario EL elemental analysis instrument (Elementar Co., Germany). Thermogravimetric (TGA) measurements were carried out with a Netzsch TG209F3 (Germany) at a heating rate of 20 °C min^{-1} under a nitrogen atmosphere. Differential scanning calorimetry (DSC) analysis was performed on a Netzsch (DSC200F3; Germany) apparatus at a heating/cooling rate of 10 °C min^{-1} under nitrogen atmosphere. UV-Vis absorption spectra were recorded on an HP 8453 spectrophotometer (USA). Cyclic voltammetry was done on a CHI660A electrochemical workstation (Shanghai Chenhua, China) with platinum electrodes at a scan rate of 50 mV s^{-1} against an Ag/Ag$^+$ reference electrode with a nitrogen-saturated solution of 0.1 mol L^{-1} tetrabutylammonium hexafluorophosphate (Bu_4NPF_6) in acetonitrile. Potentials were referenced to the ferrocenium/ferrocene couple by using ferrocene as an internal standard. The deposition of a copolymer on the electrode was done by the evaporation of a dilute THF solution. Tapping-mode atomic force microscopy (AFM) images were obtained using a NanoScope NS3A system (Digital Instruments, USA) to observe the surface morphology. The work function was determined by the scanning Kelvin probe system SKP 5050 (KP Technology, England).

2.2 Synthesis of monomers and polymers

2.2.1 (4-Fluorophenyl)(thiophen-2-yl)methanone (**1**)

Thiophene (8.4 g, 100 mmol), 4-fluorobenzoyl chloride (15.9 g, 100 mmol) and dichloromethane (100 mL) were put into a 500 mL flask. Aluminum chloride (14.0 g, 105 mmol) was added in small portions within 1 h; the reactant was kept below 10 °C by an ice water bath. The dark-red mixture was stirred at room temperature for 1 h after the addition. The sticky reactant was poured into a mixture of 200 g ice and 50 mL concentrated hydrochloride acid, and then the organic phase was washed several times with water. The combined organic layers were dried over anhydrous $MgSO_4$ and filtered and concentrated by vacuum evaporation. Compound **1** (18.9 g, 92%) was obtained as a dark brown solid that could be used in the next step without any further purification. ^{1}H NMR (600 MHz, $CDCl_3$), δ (ppm): 7.92–7.89 (m, 2H), 7.73–7.72 (m, 1H), 7.63–7.62 (m, 1H), 7.19–7.16 (m, 3H).

2.2.2 (4,5-Bis(chloromethyl)thiophen-2-yl)(4-fluorophenyl)-methanone (**2**)

Compound **1** (15.2 g, 73.7 mmol) and chloromethyl methyl ether (29.7 g, 368.5 mmol) were mixed in a 250 mL flask cooled by an ice bath; titanium tetrachloride (21.0 g, 110.6 mmol) was added dropwise within 30 min. After removal from the ice bath, the reactant was stirred under ambient temperature for 1 h and then heated to 50–60 °C and stirred for 6 h. Next, the sticky reactant was poured into 300 g cracked ice and extracted by diethyl ether. After removal of the volatile solvent, the dark brown solid (11 g, 50%), Compound **2**, was used without any purification. ^{1}H NMR (300 MHz, $CDCl_3$), δ (ppm): 8.07–7.86 (m, 2H), 7.60 (s, 1H), 7.23–7.15 (m, 2H), 5.29 (s, 2H), 4.61 (s, 2H).

2.2.3 (4,6-Dihydrothieno[3,4-*b*]thiophen-2-yl)(4-fluorophenyl)methanone (**3**)

The dark brown solid Compound **2** (10.2 g), was dissolved into 1 L slightly boiling methanol, then a solution of sodium sulfide (9.6 g, 60% content, 40 mmol) in 250 mL methanol was added dropwise within 1 h at boiling temperature. The reactant was kept at boiling temperature for 1 h. Methanol was removed by rotary evaporation; next, the sticky residue was absorbed by silica gel. The crude product was purified by silica-gel chromatography using dichloromethane/petroleum ether (1:4, *v*/*v*) as eluent to afford Compound **3** (1.93 g, 22%) as light yellow solids. ^{1}H NMR (300 MHz, $CDCl_3$), δ (ppm): 7.91–7.85 (m, 2H), 7.31 (s, 1H), 7.21–7.14 (m, 2H), 4.24 (s, 2H), 4.07 (s, 2H). Anal. calcd. (%) for $C_{13}H_9FOS_2$: C 59.07; H 3.43; S 24.26. Found: C 59.52; H 3.01; S 23.87.

2.2.4 (4-Fluorophenyl)(thieno[3,4-*b*]thiophen-2-yl)methanone (**4**)

Compound **3** (1.73 g, 6.6 mmol) was dissolved into 50 mL chloroform and cooled down to –40 °C by aliquid nitrogen/ethyl acetate bath, after which *m*-chloroperoxybenzoic acid (*m*-CPBA) (1.14 g) in chloroform (20 mL) was added dropwise. After being stirred at –40 °C for 30 min, the reactant was warmed up to ambient temperature and stirred

overnight. The chloroform was removed by rotary evaporation under vacuum, after which 15 mL acetic acid anhydride was added and the mixture was refluxed for 1 h. After removal of the volatile substance by rotary evaporation under vacuum, the residue was purified by silica-gel chromatography using dichloromethane/petroleum ether (1:4, *v*/*v*) as eluent to afford Compound **4** (1.21 g, 70%) as light yellow solids. ^{1}H NMR (300 MHz, $CDCl_3$), δ (ppm): 7.94–7.88 (m, 2H), 7.68–7.66 (d, *J*=6.0 Hz, 1H), 7.49–7.48 (d, *J*=3.0 Hz, 1H), 7.34–7.33 (d, *J*=3.0 Hz, 1H), 7.22–7.19 (m, 2H). Anal. calcd. (%) for$C_{13}H_7FOS_2$: C 59.52; H 2.69; S 24.45. Found: C 60.04; H 2.87; S 22.95.

2.2.5 (4,6-Dibromothieno[3,4-*b*]thiophen-2-yl)(4-fluorophenyl)methanone (**5**)

Compound **4** (1.94 g, 4.6 mmol) was dissolved in 15 mL DMF. Under the protection of inert atmosphere, NBS (2.05 g, 11.5 mmol) was added in one portion. The reactant was stirred for 3 h and then poured into 50 mL of 5% sodium thiosulfate solution with ice. The mixture was extracted by diethyl ether. After removal of the volatile substance by rotary evaporation under vacuum, the residue was purified by silica-gel chromatography using dichloromethane/petroleum ether (1:5, *v*/*v*) as eluent to afford Compound **5** (1.55 g, 80%) as light green solids; these were crystallized from ethanol to obtain light green needle-like crystals. ^{1}H NMR (300 MHz, $CDCl_3$), δ (ppm): 7.93–7.90 (m, 2H), 7.31 (s, 1H), 7.25–7.19 (m, 2H). Anal. calcd. (%) for $C_{13}H_5Br_2FOS_2$: C 37.17; H 1.20; S 15.26. Found: C 37.86; H 1.35; S 14.79.

2.2.6 Polymerization of PBDT-T6-TTF

BDT-T6 (0.126 g, 0.3 mmol) or BDT-T12 (0.304 g, 0.3 mmol) was dissolved into 6 mL toluene/DMF (8:1, *v*/*v*) in a flask protected by argon. The solution was flushed by argon for 10 min, then 10 mg of $Pd(PPh_3)_4$ was added into the flask. The solution was flushed again by argon for 20 min. The oil bath was gradually heated to 110 °C, after which the reactant was stirred for 48 h at 110 °C under argon atmosphere. The mixture was then poured into methanol under vigorous stirring. The precipitated solid was filtered and washed first with acetone and second with hexane to remove oligomers and catalyst residues. The dark polymer powder was dried under vacuum at 50 °C for 2 d to give 228 mg of the final product (80%). GPC: M_w=20.9 kg mol^{-1}; M_w/M_n=1.64. ^{1}H NMR ($CDCl_3$, 600 MHz), δ (ppm): 8.00–7.99 (m, 2H), 7.88–7.81 (m, 2H), 7.71–7.65 (m, 2H), 7.38 (s, 1H), 7.22–7.20 (m, 2H), 2.90–2.83 (m, 4H), 2.69–2.61 (m, 4H), 1.58–1.38 (m, 32H), 0.93–0.87 (m, 12H). Anal. calcd. (%) for $(C_{55}H_{61}FOS_6)_n$: C 69.58; H 6.68; S 20.26. Found: C 68.15; H 6.29; S 19.51.

2.2.7 Polymerization of PBDT-T12-TTF

When Compound **7** was used instead of Compound **6**, the dark polymer powder PBDT-T12-TTF with a yield of 80% was obtained. GPC: M_w=70.3 kg mol^{-1}; M_w/M_n=1.41. ^{1}H NMR ($CDCl_3$, 600 MHz), δ (ppm): 8.00–7.94 (m, 2H), 7.86–7.78 (m, 2H), 7.71–7.65 (m, 2H), 7.38 (s, 1H), 7.22–7.20 (m, 2H), 2.87–2.84 (m, 4H), 2.64–2.61 (m, 4H), 1.77–1.70 (m, 8H), 1.25–1.18 (m, 72H), 0.85–0.81 (m, 12H). Anal. calcd. (%) for $(C_{79}H_{109}FOS_6)_n$: C 73.77; H 8.70; S 14.96. Found: C 73.72; H 8.34; S 15.07.

2.3 Fabrication and characterization of solar cells

The device structure was ITO/PFN/Polymer:$PC_{71}BM$(1:1.5 by weight)/MoO_3/Al. Patterned indium tin oxide (ITO)-coated glass with a sheet resistance of 15–20 ohm/square was cleaned by a surfactant scrub and then underwent a wet-cleaning process inside an ultrasonic bath that began with deionized water, followed by acetone and 2-propanol. A thin cathode interlayer PFN of 10 nm was spin-cast onto the ITO substrate and then dried by baking in the N_2 glove box at 100 °C for 5 min. The active layer based on PBDT-T6-TTF:$PC_{71}BM$ and PBDT-T12-TTF:$PC_{71}BM$, with a thickness of 80 nm, was then deposited on top of the PFN interlayer by casting from a chlorobenzene solution or a mixed solvent of chlorobenzene/1,8-diiodoctane (97:3% by volume) and then kept overnight under vacuum. The thickness of the active layer was verified by a surface profilometer (Tencor Alpha-500, USA). A 10 nm MoO_3 layer and a 100 nm Al layer were subsequently evaporated through a shadow mask to define the active area of the devices (~2 nm×8 mm) and form a top anode. All of the fabrication processes were performed inside a controlled atmosphere of nitrogen dry box (Vacuum Atmosphere, USA) that contained less than 10 ppm oxygen and moisture. The power conversion efficiencies of the resulting polymer solar cells were measured under 1 sun, AM 1.5G (air mass 1.5 global) spectrum from a solar simulator (Oriel model 91192, USA) set to 100 mW cm^{-2}. The *J*-*V* characteristics were recorded with a Keithley 2410 source unit (USA). The external quantum efficiencies of the conventional solar cells were measured with a commercial photo modulation spectroscopic setup that included a xenon lamp, an optical chopper, a monochromator, and a lock-in amplifier operated by a PC computer. A calibrated Si photodiode was used as a standard.

2.4 Space charge-limited-current (SCLC) measurement

Hole-only devices were fabricated to measure the hole mobility using an SCLC method with a device configuration of ITO/PEDOT:PSS/Copolymer:$PC_{71}BM$/MoO_3/Al. The mobility was determined by fitting the dark current to the model of a single carrier SCLC. The detailed calculation could be found in a previous report [13].

3 Results and discussion

3.1 Synthesis and characterization

The benzoyl-substituted TT (TTF), a new 2D monomer **5** of TT, was readily synthesized from the modified procedure according to theliterature [6]; the synthesis route is shown in Scheme 1. Compound **1** was synthesized from the commercial thiophene and 4-fluoro-benzoyl chloride with a high yield of 92%. Chloromethylation of Compound **1** gave Compound **2** and then Compound **3** was achieved by the formation of thioether. Compound **4** was obtained through the following dehydrogenation. Finally, monomer **5** was successfully synthesized by the direct bromination using NBS. The two conjugated copolymers PBDT-T6-TTF and PBDT-T12-TTF were prepared by palladium (0)-catalyzed Stille coupling reactions with an equal molar ratio of monomer **5** to BDT-T6 or BDT-T12, respectively.

Polymers PBDT-T6-TTF and PBDT-T12-TTF were readily soluble in common solvents such as tetrahydrofuran (THF), chloroform, toluene, chlorobenzene, and dichlorobenzene. The molecular weights and elemental analyses of the polymers are listed in Table 1. The M_w values of PBDT-T6-TTF and PBDT-T12-TTF were 20.9 and 70.3 kg mol^{-1}, respectively, with corresponding polydispersity indices (M_w/M_n) of 1.64 and 1.41. Elemental analysis indicated that C, H, and S contents of the two copolymers were very close to those calculated from the feed compositions. Thermal stability of the polymers was investigated with TGA (Figure 1). Polymer PBDT-T6-TTF and PBDT-T12-TTF possessed decomposition temperatures of 419 °C and 388 °C, respectively, which suggested good thermal stability. No peaks associated with crystallization/melting transitions of the polymers were detected by DSC analyses, probably due to the high backbone rigidity.

3.2 Electrochemical properties

The HOMO levels of the copolymers (Table 2) were obtained from the onsets of the oxidation potentials during the cyclic voltammetry (CV) measurement. The corresponding CV spectra are shown in Figure 2. Polymers PBDT-T6-TTF and PBDT-T12-TTF showed reversible oxidations during the CV scans. The HOMO level of PBDT-T6-TTF was –5.38 eV and that of PBDT-T12-TTF was slightly lower at –5.51 eV. The dual 2D substitutions on the BDT-TT repeating

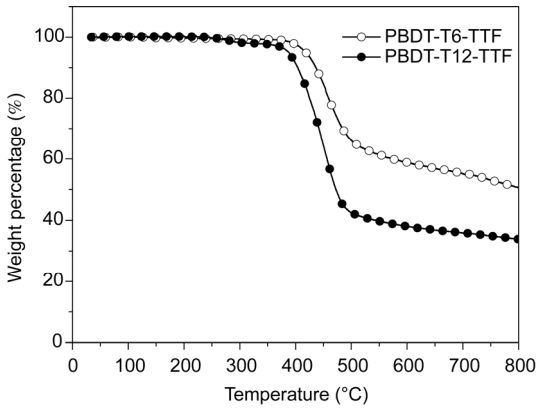

Figure 1 TGA curves of PBDT-TT6-TTF and PBDT-T12-TTF with a heating rate of 20 °C/min under nitrogen.

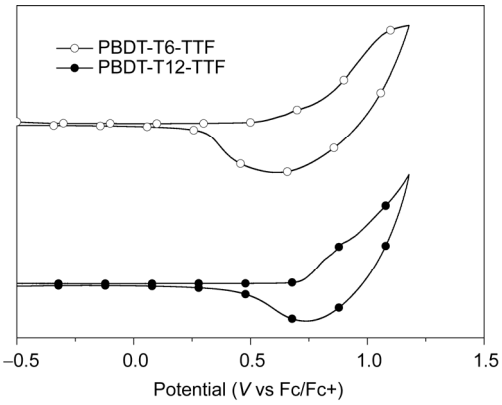

Figure 2 Cyclic voltammograms of PBDT-T6-TTF and PBDT-T12-TTF films.

Table 1 Molecular weights, elemental analyses, and decomposition temperatures of PBDT-T6-TTF and PBDT-T12-TTF

Polymer	M_w (kg mol^{-1}) [a]	M_w/M_n [a]	Elemental analysis [b]			T_d (°C) [c]
			C	H	S	
PBDT-T6-TTF	20.9	1.64	68.15 (69.58)	6.29 (6.68)	19.51 (20.26)	419
PBDT-T12-TTF	70.3	1.41	73.72 (73.77)	8.34 (8.70)	15.07 (14.96)	388

a) Estimated by GPC in THF on the basis of a polystyrene calibration; b) data given in the parentheses are contents in the feed compositions; c) temperature for 5% weight loss measured by TGA at a heating rate of 20 °C min^{-1} under nitrogen.

Table 2 Optical band gaps, electrochemical properties, and SCLC hole mobilities of PBDT-T6-TTF and PBDT-T12-TTF

Copolymer	Optical band gap (eV) [a]	E_{ox} (V)	HOMO (eV) [b]	LUMO (eV) [c]	Mobility (cm^2 V^{-1} s^{-1})
PBDT-T6-TTF	1.52	0.58	–5.38	–3.86	3.0×10^{-4}
PBDT-T12-TTF	1.54	0.71	–5.51	–3.97	1.6×10^{-5}

a) Estimated with the absorption edges of thin solid films; b) calculated according to HOMO=–e(E_{ox}+4.8); c) calculated from the HOMO level and optical bandgap.

units resulted in the lower HOMO levels [22,29]. The LUMO levels of the BDT-based copolymers were obtained from the corresponding optical band gaps and HOMO levels. The calculated LUMO levels for PBDT-T6-TTF and PBDT-T12-TTF were –3.86 eV and –3.97 eV, respectively.

3.3 Absorption spectra

The normalized UV–vis absorption spectra of PBDT-T6-TTF and PBDT-T12-TTF in THF solutions are shown in Figure 3(a). From 300 nm to 550 nm, the two polymers displayed similar absorption styles, with near ultraviolet peaks at ~327 nm and relatively weaker absorptions at ~457 nm. However, their absorptions at longer wavelengths were quite different. PBDT-T6-TTF showed a main peak at 700 nm and a shoulder peak at 648 nm, whereas the main and shoulder peaks for PBDT-T12-TTF were respectively located at 633 nm and 693 nm. These results indicate that the PBDT-T6-TTF polymer chains in the THF solution are more likely to form aggregates, in part because PBDT-T6-TTF comprises shorter alkyl side chains on the 2D BDT units.

Figure 3(b) shows the absorption coefficient spectra of PBDT-T6-TTF and PBDT-T12-TTF films on quartz substrates. The shorter wavelength range absorptions for the films of the two polymers were very close to those of their solutions, despite the films' very limited red-shifts (within 10 nm). In comparison to the solution absorptions, the films of the two polymers displayed flat absorption bands that had fewer vibronic features at longer wavelengths. Generally, the main peaks for PBDT-T6-TTF and PBDT-T12-TTF were respectively located at 705 nm and 670 nm. Figure 2(b) also shows that the absorption coefficients of PBDT-T6-TTF film were much larger than those of PBDT-T12-TTF film in the whole absorption range, which demonstrates that the shorter alkyl chain on the 2D BDT units enhanced the absorbance of a polymer film for a given thickness. In comparison with the maximum absorption coefficient, the value of 4.5×10^4 cm^{-1} for PBDT-T6-TTF was more than twice as high as that of PBDT-T12-TTF (1.96×10^4 cm^{-1}). These results suggest that too-long alkyl chains (dodecyl group) on the 2D BDT units would be harmful for the absorption of photons, an effect that is also detrimental to the realization of high photocurrent in PSCs.

The optical band gaps (E_g) for PBDT-T6-TTF and PBDT-T12-TTF calculated from the onset wavelengths of the film absorption spectra were 1.52 eV and 1.54 eV, respectively (Table 2).

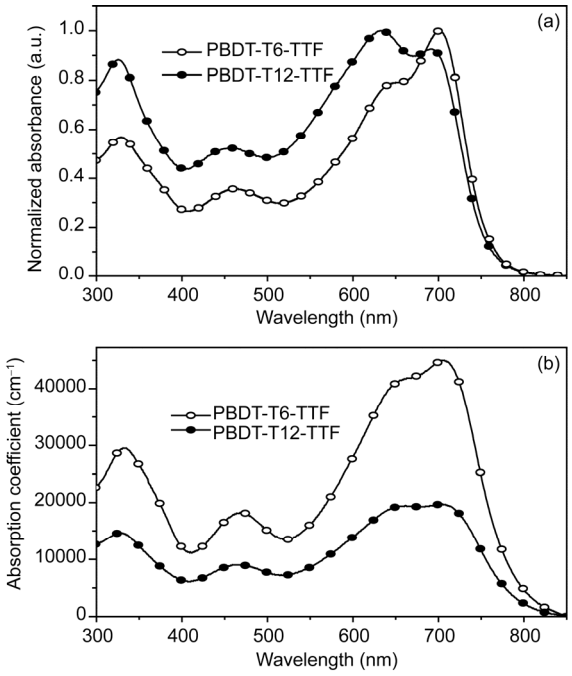

Figure 3 (a) Normalized UV-vis absorption spectra of THF solutions and (b) absorption coefficient spectra of thin solid films of PBDT-T6-TTFand PBDT-T12-TTF.

3.4 SCLC measurement

Carrier transport in polymer solar cells is more related to the transportation in the vertical direction, which can be obtained by space-charge limited current (SCLC) measurement. Hole-only devices were fabricated to measure the SCLC hole mobility (μ_{SCLC}) for the pristine polymer films. The J-V curves are shown in Figure 4 and the resulting data are listed in Table 2. PBDT-T6-TTF showed a μ_{SCLC} value of 3.0×10^{-4} cm^2 V^{-1} s^{-1}, one order of magnitude higher than the 1.6×10^{-5} cm^2 V^{-1} s^{-1} for PBDT-T12-TTF, which indicates that PBDT-T6-TTF would be better for the charge transport in polymer solar cell.

3.5 Photovoltaic performance

Taking advantage of the relatively stable configuration [31–34], we chose inverted-structure PSCs to characterize the photovoltaic performances of the dual 2D conjugated

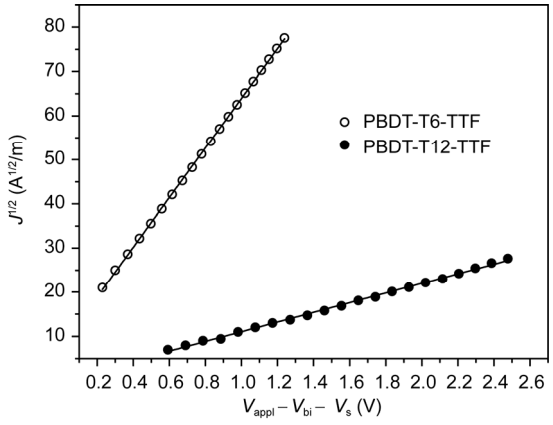

Figure 4 Experimental (symbols) and calculated (solid lines) *J*-*V* characteristics of ITO/PFN/Blend film/MoO_3 (10 nm)/Al devices with thickness *L*=80 nm and 110 nm.

copolymers. After a thin layer (10 nm) of PFN was applied on top of the ITO, the work function of the ITO was reduced from 4.7 to 4.1 eV. Clearly, the modified ITO can form ohmic contact with the photoactive layer and can therefore be used as a cathode for inverted-structure PSCs to facilitate transport and collection of photogenerated charge carriers. We also selected the MoO_3(10 nm)/Al (100 nm) as the highly reflective bilayer anode for the constructions of solar cells with a device configuration of ITO/PFN(10 nm)/(Polymer:$PC_{71}BM$=1:1.5)(80 nm)/MoO_3(10 nm)/Al(100 nm). The blend ratio of 1:1.5 for the active layer showed the best efficiency for PBDT-T6-TTF and PBDT-T12-TTF.

The measurements of the photovoltaic performances of the 2D conjugated copolymers as donors in the BHJ PSCs were performed under the illumination of an AM 1.5G simulated solar light at 100 mW cm^{-2}. The *J-V* characteristics of the BHJ PSCs are shown in Figure 5(a), and their solar cell parameters are listed in Table 3. The device based on polymer PBDT-T6-TTF exhibited an open-circuit voltage (V_{oc}) of 0.85 V. The measured short-circuit current (J_{sc}) and fill factor (FF) of the device were 8.7 mA cm^{-2} and 38.4%, respectively, which resulted in a PCE of 2.86%. The device based on PBDT-T12-TTF showed a higher V_{oc} of 0.89 V, which was in agreement with a lower HOMO level. However, the device displayed a lower J_{sc} of 5.20 mA cm^{-2} and a FF of 36.0%, which gave a lower PCE of 1.67%. The much lower J_{sc} of the PBDT-T12-TTF-based device should be partly related to the lower hole mobility of the polymer. To improve the morphology of the active layer, several additives have been widely utilized by many research groups [35–37]. In this work, we utilized 1,8-diiodooctane (DIO) as the additive (the corresponding results are listed in the Table 3). As expected, the performance of the PBDT-T6-TTF-based device was greatly improved, with a slightly lower V_{oc} of 0.82 V, a larger J_{sc} of 10.8 mA cm^{-2}, and a much higher FF of 54.9%. The PCE was remarkably elevated to 4.85%. Surprisingly, for PBDT-T12-TTF, the photovoltaic performance of the device was not improved in the presence of the DIO because of nearly unchanged V_{oc}, significantly decreased J_{sc}, and slightly increased FF. As a result, a worse PCE of 0.91% was achieved.

The external quantum efficiency (EQE) curves of the solar cells are shown in Figure 5(b). Without the DIO, the respective maxima of the two EQE curves were within 39.6% and 32.9% for PBDT-T6-TTF and PBDT-T12-TTF. With the DIO, the maximum EQE of PBDT-T6-TTF was increased to 45.9%, which could match the slight increase of J_{sc}. The PBDT-T12-TTF-based solar cell with 3% DIO showed a very low maximum EQE of 13.7%, which agreed well with the obviously decreased J_{sc}. In general, the wide EQE characteristics of the solar cells followed the wavelength range of the UV-Vis absorption spectra of the BDT-based copolymers, where $PC_{71}BM$ absorption to solar light also obviously contributed to the EQE curves.

In the presence of DIO, the change in device efficiency mainly arose from the different J_{sc} and FF. Therefore, it is essential to explore the morphology of the blend film to

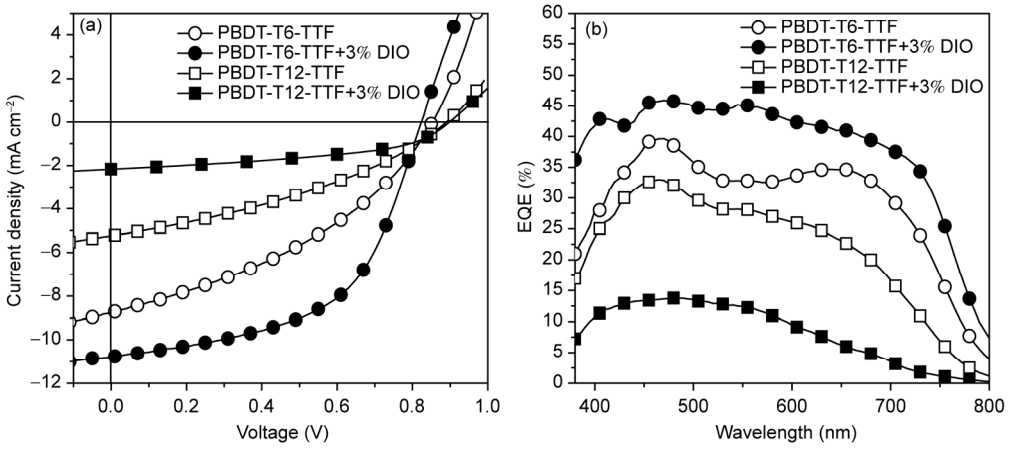

Figure 5 (a) *J-V* and (b) EQE curves of solar cells based on PBDT-T6-TTF and PBDT-T12-TTF (under illumination of AM1.5G at 100 mW cm^{-2}).

Table 3 Photovoltaic performances of the PSCs based on polymer:$PC_{71}BM$ blends

Polymer	DIO	V_{oc} (V)	J_{sc} (mA cm^{-2})	FF (%)	PCE (%) [a]
PBDT-T6-TTF	NO	0.85	8.70	38.4	2.86 (2.69)
	3%	0.82	10.8	54.9	4.85 (4.78)
PBDT-T12-TTF	NO	0.89	5.20	36.0	1.67 (1.56)
	3%	0.90	2.20	46.8	0.91 (0.88)

a) The data in parentheses are the averaged values based on more than five devices.

gain insight on its microstructure. AFM was applied to reveal the morphology of the active-layer surface. The AFM topographic images of the blend film are shown in Figure 6. As shown in Figure 6(a), the blend film based on PBDT-T6-TTF and $PC_{71}BM$ formed continuous phase separation but the extent of the two-phase separation is not obvious. With 3% DIO as the solvent additive, the domain size of phase separation of the blend film became larger and clearer (Figure 6(b)), consistent with the improved J_{sc} and FF. For PBDT-T12-TTF-based blend films (Figure 6(c)), the blend film morphology without DIO displayed individual cell-like dispersion. In addition, the large domain size might be detrimental to charge generation and this effect probably decreased the J_{sc}. When adding 3% DIO as the solvent additive, the PBDT-T12-TTF-based blend film exhibited some pits on the surface (Figure 6(d)). These pit areas generated very poor surface uniformity for the PBDT-T12-TTF-based blend film. The much lower J_{sc} of the PBDT-T12-TTF-based device may suggest poor charge separation. These effects would inevitably deteriorate its photovoltaic performance. The cell-like morphology in Figure 6(c) and the DIO caused unwanted pits (Figure 6(d)) which also indicate that the longer alkyl chains in the PBDT-T12-TTF are not suited to establish an ideal interpenetrating network between the polymer phase and $PC_{71}BM$ phase. On the basis of the morphology study, the behaviors of the blend films of the two BDT-TT-based polymers are distinctly different from one another, which suggests that the shorter alkyl chain on the 2D side chain may be more useful for the photovoltaic application of BDT-TT-based polymer donors.

Among the reported BDT-TT related polymers, PTB7 derivatives with two alkoxy/alkyl substitutions on the BDT moiety and direct flurination on the TT have shown remarkably high efficiency [10,38]. The highest PCE of 4.85% obtained with the dual 2D BDT-TT-based polymers is lower than those of the PTB7 derivatives. In this work, the thiophene-expanded 2D BDT unit comprises four alkyl groups. In combination with the fluorinated benzene-expanded 2D TT unit, the dual 2D BDT-TT-based polymers may be less coplanar along the polymer backbone, which would result in less packing ability. Even for PBDT-T6-TTF, the absorption coefficient for its film is 2.25 times lower than that of a PTB7 derivative [38]. Thus, in comparison to the PTB7 derivatives, the structural nature of the dual 2D BDT-TT-based polymers should be responsible for their lower J_{sc} and FF despite the higher V_{oc} that could be obtained by the dual 2D BDT-TT-based polymers.

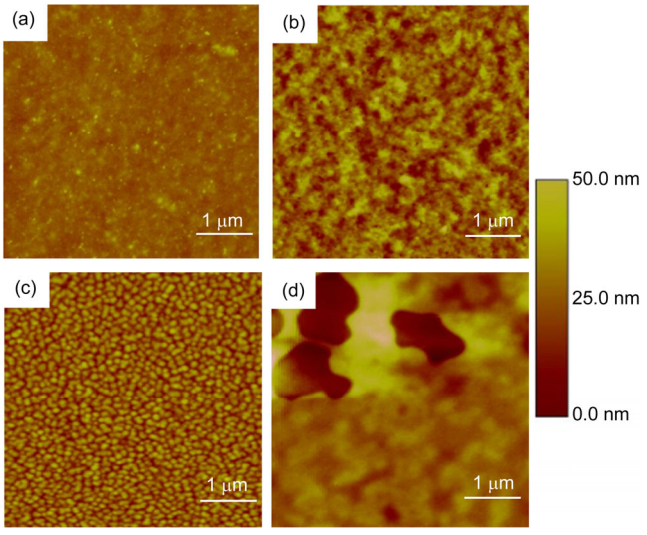

Figure 6 Tapping-mode AFM images of (a) PBDT-T6-TTF, (b) PBDT-T6-TTF add 3% DIO, (c) PBDT-T12-TTF, and (d) PBDT-T12-TTF add 3% DIO films.

4 Conclusions

With the application of the dual 2D side-chains on the BDT-TT repeating unit, two new polymers PBDT-T6-TTF and PBDT-T12-TTF were successfully synthesized. The two polymers exhibited broad absorption bands with comparable optical band gaps of ~1.53 eV. The dual 2D substitutions resulted in lower HOMO levels of –5.38 and –5.51 eV for PBDT-T6-TTF and PBDT-T12-TTF, respectively, which contributed to PCSs with high V_{oc} between 0.82 and 0.9 V. In comparison to PBDT-T12-TTF, the film of PBDT-T6-TTF with shorter alkyl-chain length possessed a much larger extinction coefficient and obviously higher SCLC hole mobility. In the absence of DIO as the solvent additive for the depositions of the blend films, PBDT-T6-TTF and PBDT-T12-TTF showed respective PCEs of 2.86% and 1.67%, mainly due to higher J_{sc} achieved by the former polymer. The blend film based on PBDT-T6-TTF showed better tunable morphology. The introduction of DIO elevated the PCE of PBDT-T6-TTF to 4.85% but showed an adverse effect for PBDT-T12-TTF. Our results suggest that the alkyl-chain length on the 2D BDT units would play an important role in determining the optoelectronic properties of the dual 2D BDT-TT-based polymers.

This work was financially supported by the National Natural Science Foundation of China (21225418 and 51173048), the National Basic Research Program of China (2013CB834705 and 2014CB643505), and GDUPS(2013).

1 Günes S, Neugebauer H, Sariciftci NS, Conjugated polymer-based organic solar cells. *Chem Rev*, 2007, 107: 1324–1338
2 Li YF, Zou YP. Conjugated polymer photovoltaic materials with broad absorption band and high charge carrier mobility. *Adv Mater*, 2008, 20: 2952–2958
3 Chen JW, Cao Y. Development of novel conjugated donor polymers for high-efficiency bulk-heterojunction photovoltaic devices. *Acc Chem Res*, 2009, 42: 1709–1718
4 Liu Z, Xu F, Yan DD. New progress in the device physics of polymer-fullerene solar cells. *Acta Chim Sinica*, 2014, 72: 171–184
5 Liang YY, Wu Y, Feng DQ, Tsai ST, Son HJ, Li G, Yu P. Development of new semiconducting polymers for high performance solar

cells. *J Am Chem Soc*, 2008, 131: 56–57
6 Hou JH, Chen HY, Zhang SQ, Chen RI, Yang Y, Wu Y, Li G. Synthesis of a low band gap polymer and its application in highly efficient polymer solar cells. *J Am Chem Soc*, 2009, 131: 15586–15587
7 Chen HY, Hou JH, Zhang SQ, Liang YY, Yang GW, Yang Y, Yu LP, Wu Y, Li G. Polymer solar cells with enhanced open-circuit voltage and efficiency. *Nat Photon*, 2009, 3: 649–653
8 Liang YY, Xu Z, Xia JB, Tsai S-T, Wu Y, Li G, Ray C, Yu LP. For the bright future—Bulk heterojunction polymer solar cells with power conversion efficiency of 7.4%. *Adv Mater*, 2010, 22: E135–E138
9 He ZC, Zhong CM, Huang X, Wong WY, Wu HB, Chen LW, Su SJ, Cao Y. Simultaneous enhancement of open-circuit voltage, short-circuit current density, and fill factor in polymer solar cells. *Adv Mater*, 2011, 23: 4636–4643
10 He ZC, Zhong CM, Su SJ, Xu M, Wu HB, Cao Y. Enhanced power-conversion efficiency in polymer solar cells using an inverted device structure. *Nat Photon*, 2012, 6: 591–595
11 Kim HJ, Lee BH, Lee KC, Kim GJ, Yu JY, Kim N, Lee SH, Lee K. Role of the side chain in the phase segregation of polymer:fullerene bulk heterojunction composites. *Adv Energy Mater*, 2013, 3: 1575–1580
12 Fan J, Yuen JD, Wang MF, Seifter J, Seo JH, Mohebbi AR, Zakhidov D, Heeger A, Wudl F. High-performance ambipolar transistors and inverters from an ultralow bandgap polymer. *Adv Mater*, 2012, 24: 2186–2190
13 Chen ZH, Cai P, Chen JW, Liu XC, Zhang LJ, Lan LF, Peng JB, Ma YG, Cao Y. Low band-gap conjugated polymers with strong interchain aggregation and very high hole mobility towards highly efficient thick-film polymer solar cells. *Adv Mater*, 2014, 26: 2586–2591
14 Lei T, Wang JY, Pei J. Roles of flexible chains in organic semiconducting materials. *Chem Mater*, 2013, 26: 594–603
15 Akkerman HB, Mannsfeld SCB, Kaushik AP, Verploegen E, Burnier L, Zoombelt AP, Saathoff JD, Hong S, Atahan-Evrenk S, Liu XL, Aspuru-Guzik A, Toney MF, Clancy P, Bao ZN. Effects of odd–even side chain length of alkyl-substituted diphenylbithiophenes on first monolayer thin film packing structure. *J Am Chem Soc*, 2013, 135: 11006–11014
16 Liang YY, Feng DQ, Wu Y, Tsai S-T, Li G, Ray C, Yu LP. Highly efficient solar cell polymers developed via fine-tuning of structural and electronic properties. *J Am Chem Soc*, 2009, 131: 7792–7799
17 Huo LJ, Hou JH, Zhang SQ, Chen HY, Yang Y. A polybenzo[1,2-b:4,5-b′]dithiophene derivative with deep HOMO level and its application in high-performance polymer solar cells. *Angew Chem Int Ed*, 2010, 49: 1500–1503
18 Huo LJ, Guo X, Zhang SQ, Li YF, Hou JH. PBDTTTZ: a broad band gap conjugated polymer with high photovoltaic performance in polymer solar cells. *Macromolecules*, 2011, 44: 4035–4037
19 Wu Y, Li ZJ, Guo X, Fan HL, Huo LJ, Hou JH. Synthesis and application of dithieno[2,3-d:2[prime or minute],3[prime or minute]-d[prime or minute]]benzo[1,2-b:4,5-b[prime or minute]]dithiophene in conjugated polymer. *J Mater Chem*, 2012, 22: 21362–21365
20 Huo LJ, Ye L, Wu Y, Li ZJ, Guo X, Zhang MJ, Zhang SQ, Hou JH. Conjugated and nonconjugated substitution effect on photovoltaic properties of benzodifuran-based photovoltaic polymers. *Macromolecules*, 2012, 45: 6923–6929
21 Ye L, Zhang SQ, Huo LJ, Zhang MJ, Hou JH. Molecular design toward highly efficient photovoltaic polymers based on two-dimensional conjugated benzodithiophene. *Acc Chem Res*, 2014, 47: 1595–1603
22 Huo LJ, Zhang SQ, Guo X, Xu F, Li YF, Hou JH. Replacing alkoxy groups with alkylthienyl groups: A feasible approach to improve the properties of photovoltaic polymers. *Angew Chem Int Ed*, 2011, 50: 9697–9702
23 Kim JH, Song CE, Kim BS, Kang I-N, Shin WS, Hwang DH. Thieno[3,2-b]thiophene-substituted benzo[1,2-b:4,5-b′]dithiophene as a promising building block for low bandgap semiconducting polymers for high-performance single and tandem organic photovoltaic cells. *Chem Mater*, 2013, 26: 1234–1242
24 Cui CH, Wong WY, Li YF. Improvement of open-circuit voltage and photovoltaic properties of 2D-conjugated polymers by alkylthio substitution. *Energy Environ Sci*, 2014, 7: 2276–2284
25 Huo LJ, Li ZJ, Guo X, Wu Y, Zhang MJ, Ye L, Zhang SQ, Hou JH. Benzodifuran-alt-thienothiophene based low band gap copolymers: substituent effects on their molecular energy levels and photovoltaic properties. *Polym Chem*, 2013, 4: 3047–3056
26 Huang Y, Huo LJ, Zhang SQ, Guo X, Han CC, Li YF, Hou JH. Sulfonyl: a new application of electron-withdrawing substituent in highly efficient photovoltaic polymer. *Chem Commun*, 2011, 47: 8904–8906
27 Wu Y, Li ZJ, Ma W, Huang Y, Huo LJ, Guo X, Zhang MJ, Ade H, Hou JH. PDT-S-T: a new polymer with optimized molecular conformation for controlled aggregation and π–π stacking and its application in efficient photovoltaic devices. *Adv Mater*, 2013, 25: 3449–3455
28 Homyak PD, Tinkham J, Lahti PM, Coughlin EB. Thieno[3,4-b]-thiophene acceptors with alkyl, aryl, perfluoroalkyl, and perfluorophenyl pendants for donor–acceptor low bandgap polymers. *Macromolecules*, 2013, 46: 8873–8881
29 Yamamoto T, Ikai T, Kuzuba M, Kuwabara T, Maeda K, Takahashi K, Kanoh S. Synthesis and characterization of thieno[3,4-b]thiophene-based copolymers bearing 4-substituted phenyl ester pendants: facile fine-tuning of HOMO energy levels. *Macromolecules*, 2011, 44: 6659–6662
30 Meager I, Ashraf RS, Mollinger S, Schroeder BC, Bronstein H, Beatrup D, Vezie MS, Kirchartz T, Salleo A, Nelson J, McCulloch I. Photocurrent enhancement from diketopyrrolopyrrole polymer solar cells through alkyl-chain branching point manipulation. *J Am Chem Soc*, 2013, 135: 11537–11540
31 Sun JM, Zhu YX, Xu XF, Lan LF, Zhang LJ, Cai P, Chen JW, Peng JB, Cao Y. High efficiency and high V_{oc} inverted polymer solar cells based on a low-lying HOMO polycarbazole donor and a hydrophilic polycarbazole interlayer on ITO cathode. *J Phys Chem C*, 2012, 116: 14188–14198
32 Yang TB, Qin DH, Lan LF, Huang WB, Gong X, Peng JB, Cao Y. Inverted polymer solar cells with a solution-processed zinc oxide thin film as an electron collection layer. *Sci China Chem*, 2012, 55: 755–759
33 Jiang ZL, Yang D, Wang N, Zhang FJ, Zhao B, Tan ST, Zhang J. Inverted polymer solar cells with TiO_2 electron extraction layers prepared by magnetron sputtering. *Sci China Chem*, 2013, 56: 1573–1577
34 Zhu YX, Xu XF, Zhang LJ, Chen JW, Cao Y. High efficiency inverted polymeric bulk-heterojunction solar cells with hydrophilic conjugated polymers as cathode interlayer on ITO. *Sol Energy Mater Sol Cells*, 2012, 97: 83–88
35 Gao L, Zhang J, He C, Zhang Y, Sun QJ, Li YF. Effect of additives on the photovoltaic properties of organic solar cells based on triphenylamine-containing amorphous molecules. *Sci China Chem*, 2014, 57: 966–972
36 Chen ZH, Cai P, Zhang LJ, Zhu YX, Xu XF, Sun JM, Huang J, Liu XC, Chen JW, Chen HZ, Cao Y. Donor–acceptor copolymers based on phenanthrene as electron-donating unit: synthesis and photovoltaic performances. *J Polym Sci Part A, Polym Chem*, 2013, 51: 4966–4974
37 Huang J, Zhu Y, Zhang LJ, Cai P, Xu XF, Chen JW, Cao Y. Low band-gap D–A conjugated copolymers based on anthradithiophene and diketopyrrolopyrrole for polymer solar cells and field-effect transistors. *J Polym Sci Part A, Polym Chem*, 2014, 52: 1652–1661
38 Liao SH, Jhuo HJ, Cheng YS, Chen SA. Fullerene derivative-doped zinc oxide nanofilm as the cathode of inverted polymer solar cells with low-bandgap polymer (PTB7-Th) for high performance. *Adv Mater*, 2013, 25: 4766–4771